Materials Science-Poland, 36(2), 2018, pp. 320-326
http://www.materialsscience.pwr.wroc.pl/
DOI: 10.2478/msp-2018-0050

DE GRUYTER OPEN

Facile microwave-assisted synthesis of Al:Mn co-doped PbI_2 nanosheets: structural, vibrational, morphological, dielectric and radiation activity studies

I.S. YAHIA[1,2], MOHD. SHKIR[1,*], V. GANESH[1], M.M. ABUTALIB[3], H.Y. ZAHRAN[1,2], S. ALFAIFY[1]

[1]Advanced Functional Materials & Optoelectronic Laboratory (AFMOL), Department of Physics, Faculty of Science, King Khalid University, P.O. Box 9004, Abha, Saudi Arabia

[2]Nanoscience Laboratory for Environmental and Bio-medical Applications (NLEBA), Semiconductor Lab., Metallurgical Lab., Department of Physics, Faculty of Education, Ain Shams University, Roxy, 11757 Cairo, Egypt

[3]Physics Department, Faculty of Science-AL Faisaliah, Campus, King Abdulaziz University, Jeddah, Saudi Arabia

Herein, we report a successful development of nano-scale pure and Al and Mn co-doped PbI_2 using facile microwave-assisted route. Structural study was done through X-ray diffraction analysis of grain size, dislocation density and lattice strain. The crystallite size was found to vary from 28 nm to 40 nm due to Al:Mn co-doping in PbI_2. The presence of various vibrational modes was confirmed by FT-IR spectroscopy and red shifting was observed in peak positions compared to the bulk. Surface morphology, examined using a scanning electron microscope, confirmed the formation of single crystal nanosheets of a thickness in the range of 10 nm to 30 nm. The single crystal nanosheets were found to be transformed to large area nanosheets due to the doping. Enhancement in dielectric constant from ∼7.5 to 11 was observed with increasing Al doping concentration. Linear attenuation coefficient was calculated and showed the enhancement of blocking gamma rays with increasing doping concentration. Its value was found to increase from 7.5 to 12.8 with the doping. The results suggest that the synthesized nanostructures can be used for detection and absorption of gamma rays emitted by ^{137}Cs and ^{241}Am sources.

Keywords: *semiconductor; scanning electron microscopy (SEM); Raman spectroscopy; dielectric properties; radiation effects*

1. Introduction

Lead iodide PbI_2 is an environmentally stable material able to absorb the radiation such as X- and γ-ray. It belongs to the wide band gap semiconductor family possessing the energy gap of 2.27 eV to 2.3 eV [1, 2], which makes it promising for low noise radiation detectors operating at room temperature [3, 4]. Besides, being used in radiation detectors, it has excellent photoluminescence [5], electrical and optical characteristics [6, 7]. It is also a promising material to be used in perovskite solar cells for advances energy conversion devices [8, 9]. Various techniques have been applied for the nanosynthesis of PbI_2 [10–13]. The structure, surface morphology and the application of the PbI_2 strongly depend on the way of its preparation [14–17]. Nano-materials have a great potential in various advanced applications [18–21].

In this research, we have synthesized pure and co-doped Al:Mn:PbI_2 nanostructures through microwave-assisted route at various percentages of Al doping. We have studied various properties of the prepared nanostructures, such as structure, morphology, dielectric and AC electrical conductivity. Moreover, to test some potential applications, we have examined the prepared nanostructures for gamma radiation and calculated the related parameters.

2. Experimental

2.1. Materials and synthesis

For the synthesis of the title nanostructures, lead acetate trihydrate, sodium iodide, poly(vinyl alcohol), cetyltrimethyl ammonium bromide,

*E-mail: shkirphysics@gmail.com

sodium iodide, aluminum nitrate nonahydrate and manganese nitrate hydrate were bought from Sigma-Aldrich and used without any further purification. Similar method has been used for the synthesis of the title materials as reported in our previous work [22]. The doping concentration of Mn was kept constant (i.e. 10 %) and for Al it was varied from 1 % to 10 % in subsequent synthesis processes.

2.2. Characterization techniques

The structural analysis of the prepared pure and Al:Mn co-doped PbI_2 nanostructures was performed through X-ray diffraction (XRD) (LabX-XRD-6000 Shimadzu). FT-Raman spectroscopy from Thermo Fisher Scientific, DXR FT-Raman spectrometer was used to study vibrational modes of PbI_2 nanostructures co-doped with Al and Mn. The surface morphological analysis was performed using a scanning electron microscope (SEM-6360-JSM) operated at 20 kV. Semiconductor characterization system 4200-SCS from Keithley was used to measure impedance, capacitance and dissipation factor of nanostructured PbI_2 co-doped with Al and Mn. From the above data, we were able to calculate the dielectric constant, dielectric loss and AC electrical conductivity of the studied materials. Thermo Scientific, DXR FT-Raman spectrometer was used to record the Raman analysis. The spectra were acquired from 1200 cm^{-1} to 50 cm^{-1}. The laser power of 0.2 mW (532 nm) was used. The dielectric and electric characteristics were measured with Keithley 4200-SCS in the frequency range from 3 kHz to 10 MHz. The radiation intensity before and after attenuation was detected through NaI detector 1.5 PX 1.5/2.0 IV (Rexon, Components, Inc., USA). The lead shield was used to protect the surroundings from radiation. To irradiate the sample, gamma ray sources Cs-137 of energy 662 keV and Am-241 of energy 59.5 keV were used at room temperature. Then, the linear absorption coefficient μ, half value thickness $X_{1/2}$, tenth value thickness $X_{1/10}$ and mean free path (MFP) were obtained for all the tested samples.

3. Results and discussion

3.1. Structural analysis

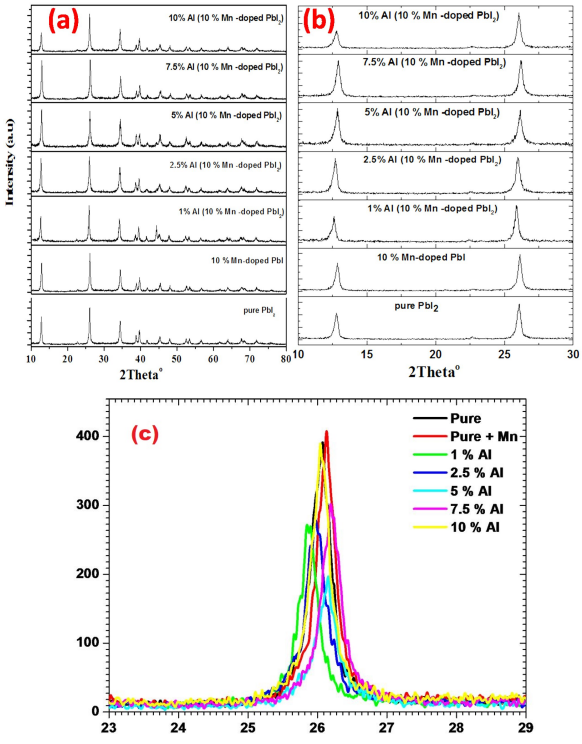

Fig. 1. (a) XRD diffraction patterns and (b) variation of intensity of (0 0 1) and (1 0 1) peaks and (c) change in peak position for pure and co-doped PbI_2 nanosheets.

The X-ray diffraction patterns of pure and co-doped with aluminum and manganese lead iodide are shown in Fig. 1a. The sharp diffraction peaks of the pure and co-doped samples indicate highly crystalline nature of the prepared samples. The prepared samples were found to be well agreed with the JCDPS Card No. 7-0235 indicating their hexagonal nature. The diffraction patterns of the studied materials were observed along the (0 0 1), (1 0 0), (0 0 2), (1 0 1), (1 0 2), (0 0 3), (1 1 0), (1 1 1), (1 0 3), (2 0 1), (0 0 4), (2 0 2), (1 1 3), (2 0 3), (2 1 1), (1 1 4), (2 1 2), (1 0 5), and (2 1 3) planes. The observed planes are consistent with previous reports on pure and doped PbI_2 nanostructures [10, 11]. We have noticed that the co-doping affected the diffraction patterns of lead iodide.

The prominent diffraction peaks occurred from 10° to 30°. Fig. 1b shows the diffraction planes of (0 0 1) and (0 0 2) for pure and Al:Mn co-doped lead iodide nanostructures for comparative study. It is clear that by varying the Al doping concentration, the intensity of planes (0 0 1) and (0 0 2) is varying. The change in the intensity and variation in the diffraction angle was observed and documented in Table 1. Also the change in peak position of higher intensity peaks due to doping is presented in Fig. 1c. The grain size of the as-prepared material was estimated by applying the Scherer equation as follows [23, 24]:

$$D = \frac{0.9\Lambda}{\beta \cos\theta} \tag{1}$$

The mean value of grain size of the pure PbI_2 was found to be 28.39 nm, while the doping of 10 % Mn has increased the grain size from 28.39 nm to 32.89 nm. We have noticed that co-doping of Al and Mn has a random effect on the grain size of pure PbI_2. The dislocation density for the prepared samples has been studied by the following relation [25]:

$$\delta = \frac{1}{D^2} \tag{2}$$

The change in the dislocation density has been concisely documented in Table 1. The lattice strain for each prepared samples was calculated by the equation:

$$\varepsilon = \beta \cos\theta / 4 \tag{3}$$

The complete structural analysis for pure and co-doped PbI_2 has been listed in Table 1, while the change in the intensity of the major planes of Al-doped 10 % Mn:PbI_2 has been described concisely in Table 2. The variation in the grain size, dislocation density and lattice strain was observed with respect to pure PbI_2.

3.2. FT-Raman spectroscopy analysis

The recorded FT-Raman spectra for the prepared nanostructures of pure and Al:Mn co-doped PbI_2 are shown in Fig. 2. The Raman spectra show the variation in the intensity for pure and co-doped PbI_2. The intensity variation attributed to the change in crystallinity and defects present in the nanostructures, could also be observed in the XRD patterns of the samples. The peak positions were observed at about 33.87 cm^{-1}, 72.40 cm^{-1}, 95.45 cm^{-1}, 109.04 cm^{-1}, 165.93 cm^{-1} and 212.22 cm^{-1} with minute variation of the peaks position assigned as E_2^1, A_1^1, A_1^2, $2E_u$, A_{2u}, $2E_2^1$ and $2E_1^1$, respectively. The vibration band around 33 cm^{-1} may be assigned to breathing motion of PbI_2 layers [10, 26]. These bands are attributed to 2H-PbI_2 nanoparticles and more details can be found in the literature [10, 16].

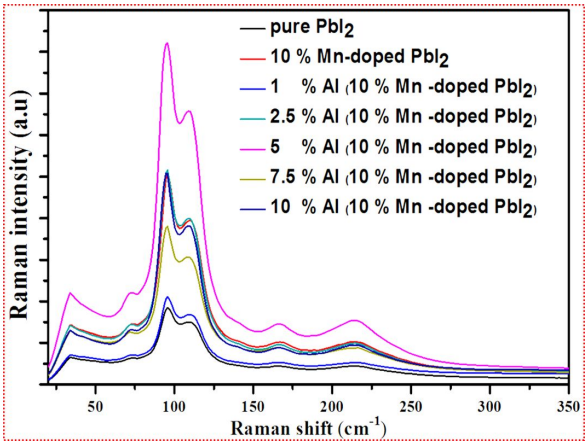

Fig. 2. Raman spectra of pure and Al:Mn co-doped PbI_2 nanosheets.

3.3. Surface morphology and EDX analysis

The surface morphology of the nanostructured material plays a crucial role in various applications such as photovoltaics [27]. The surface morphology of the pure and co-doped with Al and Mn PbI_2 has been shown in Fig. 3I. The doping concentration for Mn was constant (i.e. 10 %) and for Al it was varied from 1 % to 10 %. The overall structure is a combination of nano- and microparticles having no well defined pattern. From the figure, it can be seen that the pure PbI_2 contains hexagonal-shape nanocrystals which were found to be turned into sheets when doped with Mn and Al both. At higher concentration doping of Al, we have observed very fine nanoparticles (Fig. 3I), which may

Table 1. The calculated structural parameters of pure and Al:Mn co-doped PbI_2 nanosheets.

Samples	Crystallite size [nm]	Dislocation density [nm^{-2}]	Lattice strain
Pure	28.39	1.37E-03	1.26E-03
10 wt.% Mn:PbI2	32.89	1.23E-03	1.14E-03
1 wt.% Al:Mn:PbI2	39.32	9.03E-04	1.03E-03
2.5 wt.% Al:Mn:PbI2	30.58	1.20E-03	1.09E-03
5 wt.% Al:Mn:PbI2	36.77	8.78E-04	9.66E-04
7.5 wt.% Al:Mn:PbI2	39.69	8.84E-04	9.51E-04
10 wt.% Al:Mn:PbI2	31.88	1.12E-03	1.08E-03

Table 2. The changes in the growth plane of pure and Al:Mn co-doped PbI_2 nanosheets.

Materials	2θ°	Intensity [a.u.]	(h k l) planes
Pure-PbI_2	12.7723	72	0 0 1
	25.56	10	0 0 2
	26.0277	100	1 0 1
10 % Mn doped PbI_2	12.8352	74	0 0 1
	25.6	9	0 0 2
	26.0982	100	1 0 1
1 % Al co-doped Mn:PbI_2	12.577	60	0 0 1
	25.8509	100	0 0 2
	26.2	12	1 0 1
2.5 % Al co-doped Mn:PbI_2	12.6764	87	0 0 1
	25.5819	19	0 0 2
	25.9563	100	1 0 1
5 % Al co-doped Mn:PbI_2	12.8355	100	0 0 1
	25.74	21	0 0 2
	26.1005	93	1 0 1
7.5 % Al co-doped Mn:PbI_2	12.903	99	0 0 1
	25.66	7	0 0 2
	26.1703	100	1 0 1
10 % Al co-doped Mn:PbI_2	12.7574	49	0 0 1
	25.42	6	0 0 2
	26.0175	100	1 0 1

be related to Al. The nanosheets formation was also reported previously for PbI_2 doped with Gd^{3+}, prepared by hydrothermal technique [11, 21]. Quantitative analysis was also carried out through the energy dispersive X-ray spectroscopy (EDS). The EDS graphical representation of the prepared material is shown in Fig. 3II.

3.4. Dielectric and AC electrical conductivity analyses

Dielectric characteristics of the nanoscale material play an important role in various advanced applications, such as optics and photovoltaics [28]. Moreover, the dielectric constants

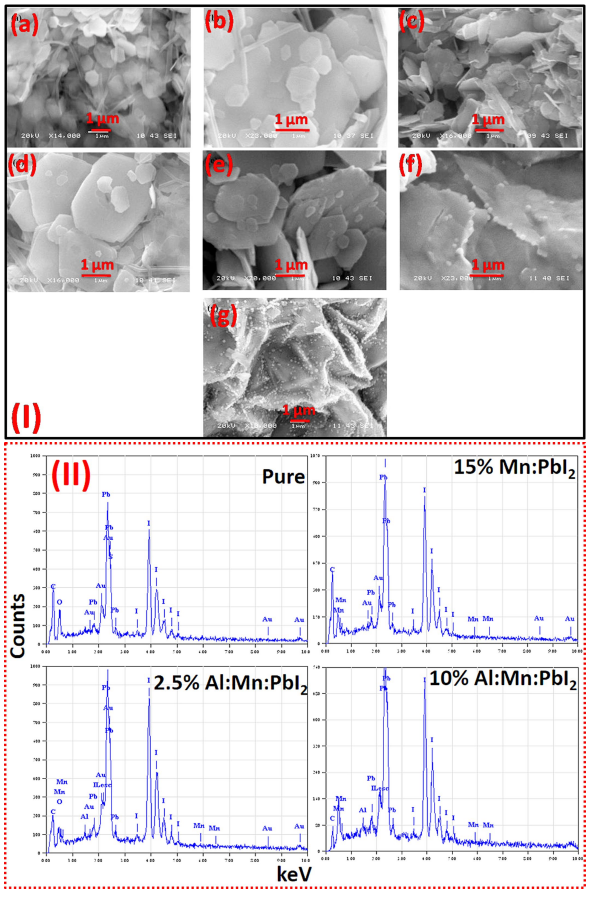

Fig. 3. (I) SEM micrograph and (II) EDX spectra of pure and Al:Mn co-doped PbI_2 nanosheets.

of the materials suggest its suitability for optoelectronics application [29]. The dielectric constants for pure and Al:Mn co-doped nanostructured PbI_2 can be characterized by the following equations [30]:

$$\varepsilon_1 = C\frac{t}{\varepsilon_o A} \tag{4}$$

$$\varepsilon_2 = \tan\delta \; x \; \varepsilon_1 \tag{5}$$

In the above equations, t is thickness and A is the area of the electrode. Fig. 4a and Fig. 4b show the dielectric constant and loss as a function of frequency, respectively. We have observed that the doping and further co-doping of the PbI_2 altered the dielectric constants. Generally, the dielectric constants were found to be stable in the entire tested range. The value of dielectric constant was

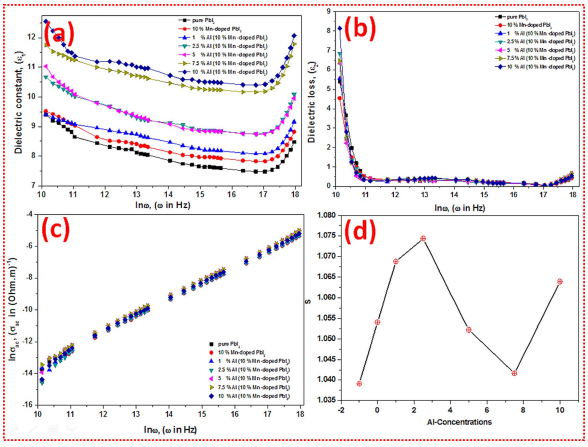

Fig. 4. (a) dielectric constant, (b) dielectric loss, (c) AC electrical conductivity and (d) frequency exponent of pure and Al:Mn co-doped PbI_2 nanosheets.

found to be enhanced with doping [22]. On comparing the dielectric results with previous reports on pure and doped nanosynthesized PbI_2, the dielectric constant value for pure PbI_2 obtained in this study was found to be about 7.5 and reached 11, when doped with Al, however, these values in our previous report on Ag:Mn:PbI_2 system were found to be nearly 8.5 and 10.5, respectively [22]. The currently calculated values were found to be lower and higher than the nano and bulk value for pure and doped PbI_2 [1, 10]. Possible reasons for low dielectric constant values are such parameters as shape, size, orientation etc. The advantage of low values of dielectric constant is that the fabricated nanosheets consume lower electrical power which is a critical factor in various device fabrications [31].

Fig. 4c shows the AC electrical conductivity σ_{ac} as a function of frequency for pure and co-doped PbI_2 nanostructures. Both the total AC electrical conductivity $\sigma_{tot.ac}$ and AC electrical conductivity σ_{ac} were calculated from the measured values of impedance Z using the following relations [32]:

$$\sigma_{tot.ac} = \frac{t}{ZA} \tag{6a}$$

$$\sigma_{ac.tot.} = \sigma_{dc} + \sigma_{ac} \tag{6b}$$

$$\sigma_{ac.tot.} = \sigma_{dc} + B\omega^s \tag{6c}$$

where t is the thicknesses and A is the area of the sample. Fig. 4c shows an increase in σ_{ac} of the pure and co-doped PbI_2 with applied frequency. The direct relation of σ_{ac} and frequency confirms that they obey the Jonscher relation (i.e. $\sigma_{ac} = B\omega^s$) [33]. The frequency exponent, s as a function of doping concentration is shown in Fig. 4d. The change in the frequency exponent might be due to the change in the ionic concentration of co-doped PbI_2 [34]. The value of s is found to be around 1 with a standard error ±0.06 for all the nanostructures.

3.5. Linear absorption coefficient analysis

The extra exposure to ionizing radiation is very dangerous to human beings; hence, it is necessary to detect such radiation present in the environment. We have applied the prepared nanoscale materials for the detection of both Cs-137 and Am-241. The linear absorption was estimated by the following equation [35]:

$$I = I_o e^{-\mu x} \tag{7}$$

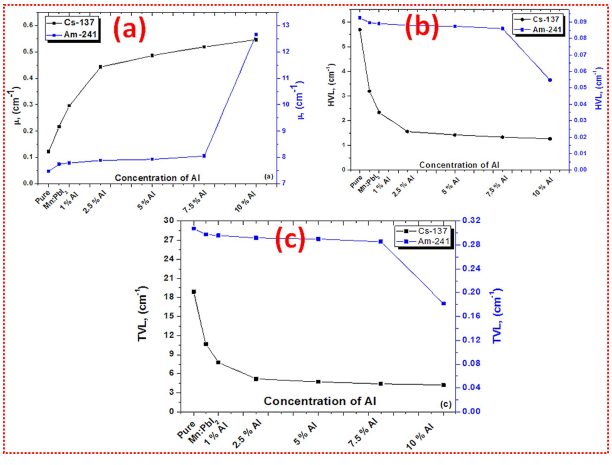

Fig. 5. (a) linear absorption coefficient, (b) HVL and (c) TVL plots of pure and Al:Mn co-doped PbI_2 nanosheets.

In equation 7, I_o is the initial intensity of radiation source, x is a thickness of the sample and μ is the linear absorption coefficient of the material. Fig. 5a shows the variation of calculated value of μ with doping concentrations of Al:Mn. It can be observed from the figure that the value of μ is enriched by doping compared to pure material which indicates that the doped nanostructures can work better as a shield material. The calculated values are found to be comparable with pure and Gd^{3+} doped PbI_2 as well as other previously reported materials [21, 35–37]. This value is also found to be higher than that in our previous system Ag:Mn:PbI_2 tested with Am-241 and published recently [22]. Furthermore, we have also calculated the values of half value layer (HVL) ($x_{1/2}$) and tenth value layer (TVL) ($x_{1/10}$), from the following equations [23, 38, 39]:

$$x_{\frac{1}{2}} = \frac{\ln 2}{\mu_l} \text{ and } x_{\frac{1}{10}} = \frac{\ln 10}{\mu_l} \tag{8}$$

The variation of the above mentioned values with doping concentration is presented in Fig. 5 from which it can be seen that the value of $x_{1/2}$ is decreasing up to some extent of doping and becomes stable for both radiation sources; the $x_{1/10}$ shows similar behavior. Such results indicate that the prepared nanostructures of Al:Mn co-doped PbI_2 can be used in radiation shielding materials at room temperature.

4. Conclusions

As a conclusion, PbI2 has been proven as a radiation detector as the co-doping of Al:Mn-enhanced its radiation detection efficiency. The increment in grain size of the prepared nanostructure material was found from 28.39 nm to 39.69 nm. The existence of nanoparticles along with sheets of micro and nanometer size was observed through scanning electron microscope. The Raman spectroscopic observation confirmed the presence of 2H polytypes of PbI_2 and were in accordance with XRD results. The dielectric constant was increased from 7.5 to 11 with increasing the dopant concentration. The conduction behavior was confirmed by AC electrical conductivity analysis. The linear absorption coefficient was found to be enriched from 7.5 to 12.8 with doping. We observed that the co-doped PbI_2 can be a good choice

as nuclear radiation detector compared to the pure one. The current research may be helpful to build the efficient radiation detectors.

Acknowledgements

The authors extend their appreciation to the Deanship of Scientific Research at the King Khalid University for funding this work through the Research Groups Program under the Grant Number R.G.P.2/9/38.

References

[1] DUGAN A., HENISCH H., *J. Phys. Chem. Solids*, 28 (1967), 971.
[2] ZHU X., WEI Z., JIN Y., XIANG A., *Cryst. Res. Technol.*, 42 (2007), 456.
[3] SILVA DA F.A., VEISSID N., VEISSID C., PEPE C., N. OLIVAIRA DE B.N., SILVA DA B.A., *Appl. Phys. Lett*, 69 (1996) 1930.
[4] CHAUDHARY S.K., *Cryst. Struct. Theor. Appl.*, 1 (2012) 21.
[5] FINLAYSON C., SAZIO P., *J. Phys. D Appl. Phys.*, 39 (2006), 1477.
[6] KLEIM R., RAGA F., *J. Phys. Chem. Solids*, 30 (1969), 2213.
[7] ANDO M., YAZAKI M., KATAYAMA I., ICHIDA H., WAKAIKI S., KANEMATSU Y., TAKEDA J., *Phys. Rev. B*, 86 (2012), 155206.
[8] QUILETTES DE D.W., VORPAHL S.M., STRANKS S.D., NAGAOKA H., EPERON G.E., ZIFFER M.E., SNAITH H.J., GINGER D.S., *Science*, 348 (2015), 683.
[9] CHEN Q., ZHOU H., HONG Z., LUO S., DUAN H.-S., WANG H.-H., LIU Y., LI G., YANG Y., *J. Am. Chem. Soc.*, 136 (2013), 622.
[10] SHKIR M., YAHIA I.S., ALFAIFY S., ABUTALIB M.M., MUHAMMAD S., *J. Mol. Struct.*, 1110 (2016), 83.
[11] SHKIR M., YAHIA I.S., GANESH V., ALGARNI H., ALFAIFY S., *Mater. Lett.*, 176 (2016), 135.
[12] GOLDBERG M., LANGER R., JIA X., *J. Biomat. Sci.-Polym. E.*, 18 (2007), 241.
[13] KLABUNDE K.J., RICHARDS R., *Nanoscale materials in chemistry*, Wiley Online Library, 2001.
[14] KAVIYARASU K., SAJAN D., SELVAKUMAR M.S., THOMAS S.A., ANAND D.P., *J. Phys. Chem. Solids*, 73 (2012), 1396.
[15] DAG I., LIFSHITZ E., *J. Phys. Chem.*, 100 (1996), 8962.
[16] KASI G.K., DOLLAHON N.R., AHMADI T.S., *J. Phys. D Appl. Phys.*, 40 (2007), 1778.
[17] ZHU G., LIU P., HOJAMBERDIEV M., ZHOU J.-P., HUANG X., FENG B., YANG R., *Appl. Phys. A-Mater.*, 98 (2010), 299.
[18] CHEN X., MAO S.S., *Chem. Rev.*, 107 (2007), 2891.
[19] ROGERS J., LAGALLY M., NUZZO R., *Nature*, 477 (2011), 45.
[20] KIM D.-H., LU N., GHAFFARI R., ROGERS J.A., *NPG Asia Mater.*, 4 (2012), e15.
[21] SHKIR M., ALFAIFY S., YAHIA I.S., GANESH V., SHOUKRY H., *Physica B*, 508 (2017), 41.
[22] YAHIA I., ABUTALIB M., *J. Mol. Struct.*, 1138 (2017), 215.
[23] YAHIA I.S., SHKIR M., ALFAIFY S., GANESH V., ZAHRAN H.Y., KILANY M., *Mat. Sci. Eng. C*, 72 (2017), 472.
[24] SHKIR M., ALFAIFY S., *Sci. Rep.*, 7 (2017), 16091.
[25] SHKIR M., KILANY M., YAHIA I.S., *Ceram. Int.*, 43 (2016), 39.
[26] CONDELES J., MULATO M., *J. Phys. Chem. Solids.*, 89 (2016), 39.
[27] AHMED W., JACKSON M.J., *Emerging nanotechnologies for manufacturing*, William Andrew, 2014.
[28] HARALD I., LÜTH H., *Solid-state physics: an introduction to principles of materials science*, Springer-Verlag, 1996.
[29] JILANI A., ABDEL-WAHAB M.S., ZAHRAN H., YAHIA I., AL-GHAMDI A.A., *Appl. Phys. A*, 122 (2016), 862.
[30] SHKIR M., ALFAIFY S., GANESH V., YAHIA I., *Solid State Sci.*, 70 (2017), 81.
[31] SHANMUGAM G., THIRUPUGALMANI K., RAKHIKRISHNA R., PHILIP J., BRAHADEESWARAN S., *J. Therm. Anal. Calorim.*, 114 (2013), 1245.
[32] KAYGILI O., DOROZHKIN S.V., ATES T., AL-GHAMDI A.A., YAKUPHANOGLU F., *Ceram. Int.*, 40 (2014), 9395.
[33] JONSCHER A.K., *Nature*, 267 (1977), 673., *Solid State Sci.*, 70 (2017), 81.
[34] JAIN V.K., VERMA A., *Physics of semiconductor devices: 17th international workshop on the physics of semiconductor devices 2013*, Springer Science & Business Media, 2013.
[35] SHAPIRO J., *Radiation protection: a guide for scientists, regulators, and physicians*, La Editorial, UPR, 2002.
[36] HUBBELL J.H., *Int. J. Appl. Radiat. Isotopes*, 33 (1982), 1269.
[37] BADRAN H., YAHIA I., HAMDY M.S., AWWAD N., *Radiat. Phys. Chem.*, 130 (2017), 85.
[38] MARTIN J.E., *Physics for radiation protection: a handbook*, John Wiley & Sons, 2006.
[39] SHKIR M., ALFAIFY S., YAHIA I.S., HAMDY M.S., GANESH V., ALGARNI H., *J. Nanopart. Res.*, 19 (2017), 328.

Received 2017-10-29
Accepted 2018-04-14